The International Journal of Advanced Manufacturing Technology (2020) 111:1333–1350
https://doi.org/10.1007/s00170-020-06184-y

ORIGINAL ARTICLE

Relationships between welding parameters, aging conditions, and weld properties in AA7075-T6 friction stir welds

D. Ambrosio[1] · C. Garnier[1] · V. Wagner[1] · E. Aldanondo[2] · G. Dessein[1] · O. Cahuc[3]

Received: 10 July 2020 / Accepted: 25 September 2020 / Published online: 11 October 2020

Abstract

The influence of processing parameters and several combinations of natural as well as artificial aging on the mechanical properties of friction stir welded AA7075-T6 is analyzed in the present investigation. Different sets of welding parameters were employed to obtain joints characterized by different peak temperatures and thermal cycles. The joint obtained with the highest welding speed has guaranteed the best mechanical properties. The latter were shown to be strongly correlated to heat input, which influences both densities of dislocations in nugget zone grains and growth and dissolution of strengthening precipitates in the heat-affected zone that establish the mechanical characteristics of friction stir welds. On the other hand, artificial aging has drastically reduced the strain at break due to strain localization in the heat affected zones while it has proved its effectiveness in stabilizing the mechanical properties when exposed to further natural aging at room temperature.

Keywords Friction stir welding · Aluminum alloys · Mechanical properties · Natural aging · Artificial aging

1 Introduction

Friction stir welding is a solid-state joining process extensively studied in the last three decades [1]. Over the years, several studies have focused on the aging of friction stir welds made with precipitation hardening aluminum alloys to study the evolution of the mechanical properties as a function of various heat treatments. The need arises from the fact that, although FSW joints have mechanical properties far superior to those obtained by other techniques [2], there are heat-affected zones that weaken the joint due to heating and cooling cycles [3]. However, the mechanical behavior of friction stir welds age-hardenable aluminum alloys is strongly influenced by the time elapsed after welding due to their dependence on natural aging [4]. Thus, it is necessary to identify suitable post-welding procedures to obtain high strength and stable properties in FSW joints to facilitate the implementation of the FSW process for manufacturing aerospace structures [5]. In early studies, Mahoney et al. [6] demonstrated that post-welding artificial aging (AA) does not affect the yield strength but decreases ductility and ultimate tensile strength in FSW AA7075-T6 joints. For the same material, Fuller et al. [7] reported the evolution of mechanical properties with natural aging (NA). The authors demonstrated the continuity of the mechanical properties' recovery process for at least up to 60,000 h after the execution of the joints. Improved mechanical properties were justified by the overall increase in the volume fraction of Guinier-Preston (GP) II within the nugget zone and HAZ and the resulting increase in hardness. However, it has been established that the kinetics of naturally aged friction stir welds is noticeable within 2 weeks after welding. Its effect is significantly reduced over longer aging periods [8]. Sato et al. [9] investigated artificial aging, solution heat treatment, and solution heat treatment followed by artificial aging for AA6063-T5. The results showed an increase in hardness with increasing artificial aging time. The combination of solution heat treatment and artificial aging has further standardized the hardness by eliminating the presence of minima, the lowest hardness values in the heat-affected zone (HAZ), that represent weak points of the joint. Similar results were observed by Jandaghi et al. [10], applying solution heat treatment and subsequent aging on

✉ D. Ambrosio
dambrosi@enit.fr

[1] Laboratoire Génie de Production (LPG), INP/ENIT 65016, Tarbes, France

[2] LORTEK Technological Centre, Basque Research and Technology Alliance (BRTA), Arranomendia Kalea 4A, 20240, Ordizia, Spain

[3] Institute of mechanics and engineering (I2M), CNRS, University of Bordeaux, 33400, Talence, France

similar and dissimilar of AA2198 and AA7475 FSW joints. Post-weld heat treatments proved to improve the hardness in AA2198 and to reduce it in AA7475. A comparison of various post-welding heat treatment (PWHT) was proposed by Sharma et al. [11]. Natural and artificial aging proved to be the most effective PWHT for improving the mechanical properties of AA7039 FSW joints.

Regardless of aging or PWHT, the mechanical properties of FSW joints are influenced by process parameters. Mishra and Komarasamy [12] showed the influence of rotational and welding speeds on the thermo-mechanical phenomena that develop during FSW and thus their impact on the final microstructure and mechanical properties of the joint. The role of welding speed in 6005A-T6 friction stir welds was investigated by Dong et al. [13]. The authors displayed that higher welding speed results in higher yield strength. Golezani et al. [14] studied the influence of rotational speed on the strength of AA7020-T6 FSW joints. The authors showed higher hardness and yield strength, but lower ductility of the joint when using low rotational speeds. Rajakumar et al. [15] highlighted the impact of rotational and welding speeds on the mechanical properties of FSW joints, while Tabasi et al. [16] proved high rotational speeds and low welding speeds promote stirring of the material. On the one hand, high welding speeds are responsible for narrow heat-affected zones, leading to high mechanical properties of the joints. On the other hand, too low rotational speeds may not ensure sufficient mixing for the mechanical bonding between the welding plates. Simultaneously, too high values may result in excessive stirring the welded material, causing flashes and/or micro-voids within the joint. Also, the influence of process parameters and different pin morphologies on the mechanical properties and corrosion of FSW joints was shown by Moharami et al. [17].

Although several works on the influence of welding parameters on the mechanical properties and the aging process in friction stir welded hardening aluminum alloys 7075 are available, an investigation combining these two factors has rarely been addressed before to the authors' knowledge [18]. For this reason, the authors have set two objectives in this study. The first is to compare the mechanical properties of the joints obtained with three different combinations of process parameters for different periods of natural aging. The second is to study the effect of PWHT on joints after an initial period of natural aging. Understanding the combination of NA and PWHT is fundamental to establishing suitable and realistic post-weld procedures in industrial manufacturing as real procedures usually combine those two phenomena due to operative reasons. The joints' mechanical properties were then evaluated directly following heat treatment and after further natural aging to see if the artificial aging was able to control the precipitation phenomenon and thus stabilize the mechanical properties of friction stir welds. Therefore, the results can clarify the influence of process parameters on mechanical properties and their evolution for different aging and the possible stabilization of mechanical properties following artificial aging.

2 Material and methods

2.1 Friction stir welding

Three bead-on-plate runs were made parallel to the rolling direction for each combination of processing parameters. The size of AA7075-T6 welding plates was 200 mm × 140 mm × 3 mm (L × W × T). The tested welding configurations and the different chosen process parameters are listed in Table 1.

The process parameters were chosen based on previous work [19] and to assess the influence of the rotational speed (WC_1) and welding speed (WC_3) against a reference configuration (WC_2). In other words, the choice was first of all driven by the willingness to analyze the influence of the maximum temperatures reached in the nugget zone (rotational speed) and the rate of thermal cycles (welding speed) on the mechanical properties and secondly by the attempt to investigate their influence on the aging process of friction stir welded joints.

The friction stir welds were performed on a Kuka KR500-3MT robot with an Actemium BPA-6700 spindle (Fig. 1). The dimensions and geometry of the tool are shown in Fig. 2a and it is characterized by grooves on the shoulder surface. As for backing plate, a 20-mm-thick mild steel was used for the tests.

Table 1 Processing parameters used in this investigation

Welding configuration	Axial force (kN)	Welding speed (mm/min)	Rotational speed (rpm)	Tilt angle (°)
WC_1	6	60	800	1.8
WC_2	5.5	60	1400	1.8
WC_3	7.5	180	1400	1.8

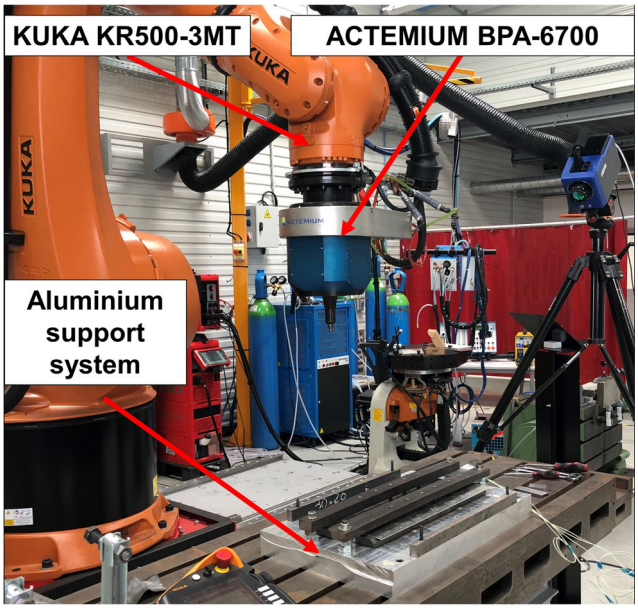

Fig. 1 Welding setup showing robot, spindle, and support system

2.2 Methods

From each joint, eight specimens for tensile tests and one specimen for metallography and microhardness test have been obtained by abrasive water jet cutting method, as shown in Fig. 2b. The specimens were stored at room temperature. Three aging conditions were tested: (i) natural aging (Nx); (ii) natural aging followed by artificial aging (NxA); (iii) natural aging followed by artificial aging, and natural aging (NxAN). The different aging conditions are summarized in Fig. 3.

The different aging conditions have been tested on all previously introduced welding configurations (Table 1). The heat treatment at 180 °C for 9 h was selected as the artificial aging as it is a commonly used PWHT in the industrial practice [20]. For each pair of process parameters and aging condition, three tensile tests and one microhardness test have been carried out.

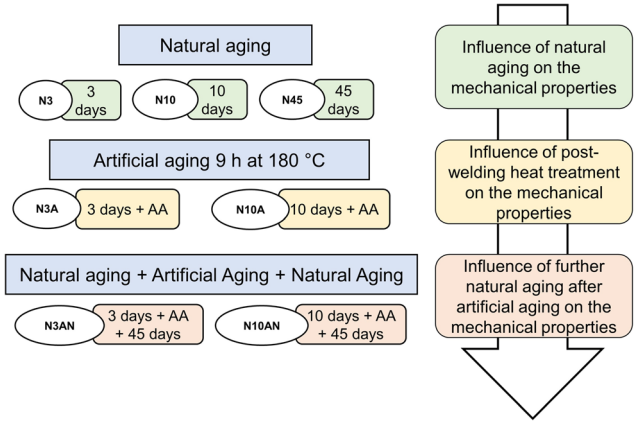

Fig. 3 Organization and labeling of the selected aging conditions

2.3 Mechanical property evaluation

Mechanical characterization of naturally and artificially aged samples was performed by tensile tests and Vickers hardness measurements. The uniaxial tensile tests have been performed using an Instron electromechanical testing machine equipped with a 100-kN load cell and cross-head speed of 1 mm/min at room temperature, following the ASTM E-8 [21] subsize specimens. The 0.2% offset yield strength Y (MPa), ultimate tensile strength UTS (MPa), and strain at break ε_b were evaluated. Strains were measured using digital image correlation (DIC) through the post-processing software Aramis.

Hardness measurements were made on polished samples using a Zwick ZHU 2,5 durometer with a load of 4.9 N and a duration time of 10 s. The hardness filiations were performed 1 mm from the samples' bottom surface to be in the center of the nugget zone. The step between the two indentations is not constant. It decreases in the transition of NZ to HAZ passing through the thermo-mechanically affected zone (TMAZ). Furthermore, it increases between HAZ and the base material (BM). Globally, sixteen points, only taken on the advancing side to reduce the execution time, are considered. A pattern of the indentation points along the weld cross-section is shown in Fig. 4.

Fig. 2 **a** Tool's information, **b** specimens' cutting scheme

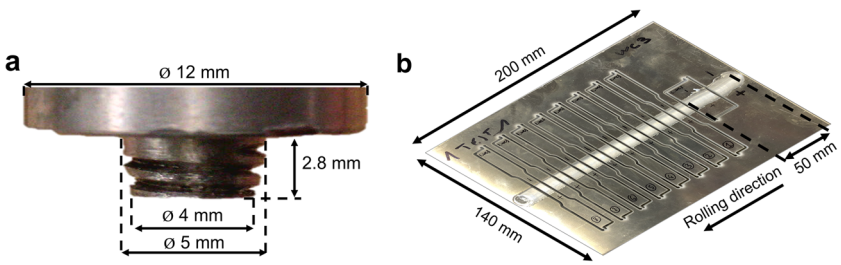

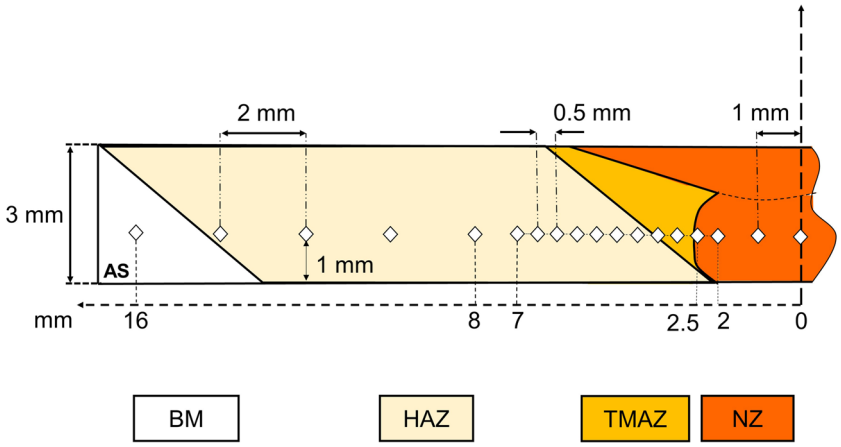

Fig. 4 Schematic representation of hardness indentations along the weld cross-section

2.4 Temperature measurements

Joints 140 mm long were repeated to perform temperature measurements in all the different welding configurations. Three K-type thermocouples measured the thermal cycle in the zones surrounding the nugget zone. The backing plate was modified to allow the placement of three thermocouples with the tip in contact with the bottom surface of the sheets in contact with the backing plate, as displayed in Fig. 5a. The distance of the thermocouples from the welding line was 3 mm (TC_1) and 7 mm (TC_3) on the retreating side (RS) and 6 mm (TC_2) on the advancing side (AS). The measurements were made at a sufficient distance from the plunging point to guarantee process stabilization.

Infrared temperature field measurements were performed with an IR camera CEDIP© Jade III MWIR retrofitted FLIR© titanium SC 7200. The IR camera placement and its position relative to the welded plates are shown in Fig. 5b. More information about the device and the setting are presented in Appendix 1.

3 Results

The analysis of the mechanical test results is divided into three parts to simplify the subsequent discussion. First of all, the results for welds underwent various natural aging period (N3, N10, N45) is detailed in subsection "Natural aging." Afterwards, the comparison between the mechanical properties of joints obtained by natural aging (N3 and N10) and those also undergone artificial aging (N3A and N10A) is outlined in subsection "Artificial aging." Lastly, the mechanical tests on specimens subjected to artificial aging and then naturally aged for 45 days (N3AN and N10AN) are presented in the "Artificial aging and natural aging" subsection. In the tensile tests analysis, only one stress-strain curve for each of the three tested samples was displayed on the graphs to facilitate their reading. The results for all the tests performed are available in Appendix 2.

3.1 Natural aging

The different combinations of process parameters have significantly influenced the mechanical properties of the joints. Figure 6a displays typical engineering stress-strain curves obtained for FSW joints obtained in WC_3 configuration and underwent the various natural aging N3, N10, and N45. Table 2 shows the results for the specimens obtained in all the welding configurations and exposed to different natural aging.

Joints obtained in the WC_3 always showed the highest UTS, Y, and ε_b when comparing specimens under the same aging conditions. Regardless of the process parameters, the mechanical properties increase progressively as the natural aging time increases, as displayed in Fig. 6a. UTS

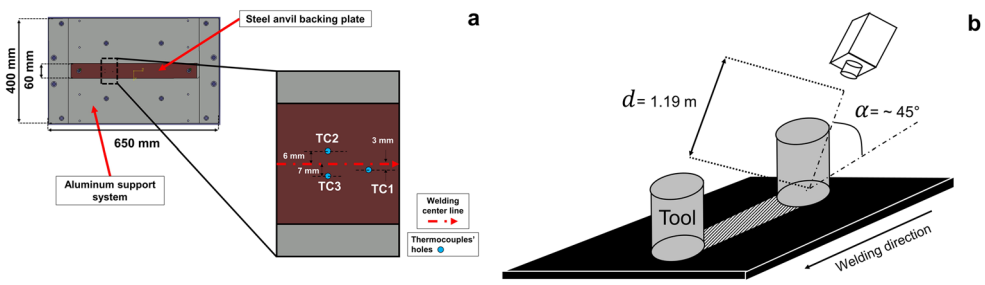

Fig. 5 **a** Position of thermocouple placement holes in the anvil, **b** position of the IR camera relative to the welding plates

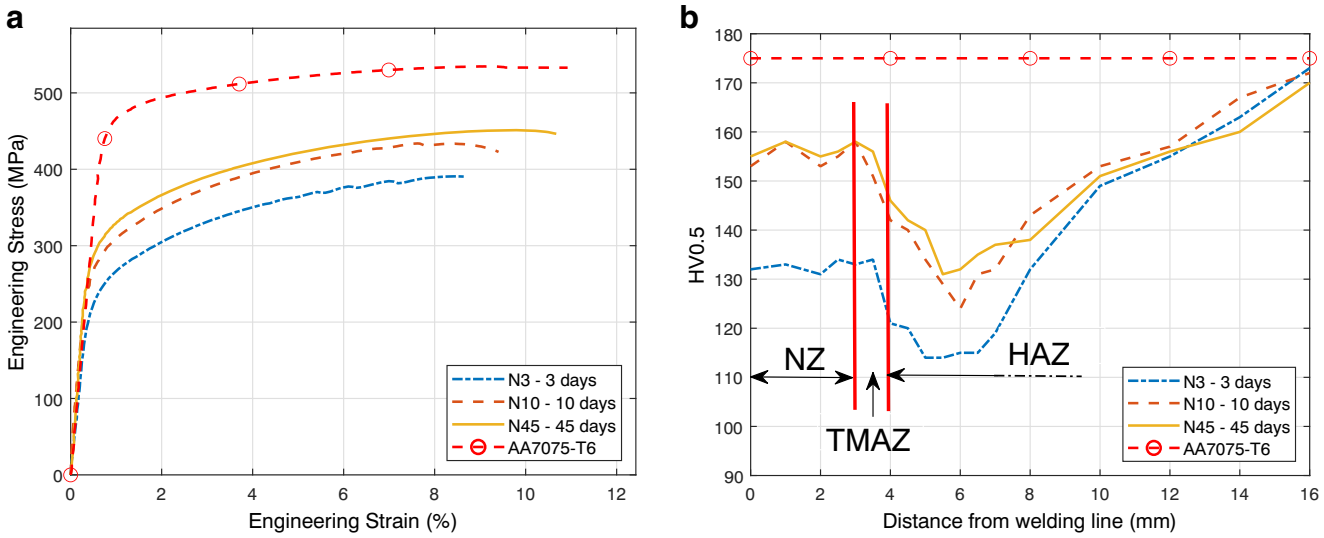

Fig. 6 **a** Engineering stress-strain curves and **b** hardness profiles for specimens N3, N10, and N45 made in the WC_3 configuration (i.e., 180 mm/min–1400 rpm–7.5 kN). Effect of the natural aging on the mechanical properties

increases on average by 15% and 3% when comparing N3-N10 and N10-N45, respectively. Contrarily, the increase in yield strength seems to be more affected by the process parameters. The biggest increase of 24% can be observed when comparing N3 and N10 in the WC_3 configuration. It is noteworthy that once yield strength is reached in all the responses, the strain hardening begins until the specimens' rupture. Also, the plastic regime has been characterized by an instability before the fracture as if it was a signal of the imminent rupture. However, it should be noted that strain at break increases with natural aging and with the reduction of the instability in the plastic regime.

The hardness profiles for welds made in the WC_3 configuration as a function of the natural aging are shown in Fig. 6b. The minimum hardness in the cross-section and the average value in the nugget zone are listed in Table 2. The average hardness value in the nugget zone was calculated by averaging the three measurements made in it (Fig. 4). It is noteworthy that after 3 days of natural aging, the average hardness in the nugget zone is almost equal for all the welding configurations, while its evolution as a function of natural aging seems to be influenced by the employed process parameters. However, regardless of the welding configuration, the largest increase in all the zones occurs between 3 and 10 days of natural aging. The minimum hardnesses are identified in the HAZ and seem to be negatively affected by the low welding speed. Focusing on WC_1 and WC_2, it is interesting to observe how both the minimum hardness in the HAZ and the average hardness value in NZ are similar and evolve almost in the same way.

The best mechanical characteristics were obtained in the configuration characterized by the highest welding speed (i.e., 180 mm/min). At the same welding speed, the different rotational speeds did not significantly change the

Table 2 Mechanical properties for naturally aged specimens fabricated with all welding configurations

WC –	T –	UTS (MPa)	Y (MPa)	ε_b (%)	HV_{HAZ} (HV0.5)	HV_{NZ} (HV0.5)
AA7075-T6		535	456	11	175	175
1	N3	340 ± 3	215 ± 4	6.8 ± 0.6	103	130 ± 1
1	N10	374 ± 5	237 ± 12	7.4 ± 0.9	111	145 ± 2
1	N45	385 ± 6	252 ± 5	7.4 ± 0.6	119	147 ± 1
2	N3	328 ± 2	195 ± 0	7.6 ± 0.1	103	131 ± 2
2	N10	376 ± 6	231 ± 8	7.2 ± 0.5	112	140 ± 2
2	N45	389 ± 3	261 ± 8	7.7 ± 0.2	115	144 ± 1
3	N3	374 ± 1	230 ± 1	8.6 ± 0.2	114	132 ± 1
3	N10	439 ± 6	286 ± 6	9.4 ± 0.7	124	155 ± 2
3	N45	449 ± 3	303 ± 1	10.6 ± 0.3	131	155 ± 1

mechanical properties of the joints showing the negligible influence of the rotational speed on the performance of a joint in the considered welding conditions. In conclusion, it is the welding speed rather than the rotational speed that mainly affects the mechanical properties of the friction stir welded joints. Regardless of the welding configuration used, from the results shown in Table 2, it is evident that the mechanical properties of the FSW joints are not stable even after 45 days of natural aging.

3.2 Artificial aging

In this section and the following one, only welds obtained in the WC_3, i.e., 180 mm/min and 1400 rpm, are reported because of their similar response to the heat treatments.

Table 3 summarizes the mechanical properties for specimens undergone by N3, N3A, N10, and N10A.

The engineering stress-strain curves in Fig. 7a show the different mechanical behavior of naturally and artificially aged joints.

The change in the mechanical behavior of FSW joints, whether or not they have undergone a post-welding heat treatment, is already clear from a simple analysis of the curves' shape. Specimens that undergo artificial aging showed a remarkable reduction higher than 50% in strain at break regardless of the previous exposure to natural aging. Comparing the engineering stress-strain curves of specimens that have undergone artificial aging, it is evident both the absence of instability in the plastic regime and the strain-softening before the fracture, both phenomena not present in specimens subjected only to natural aging. UTS and Y evolve differently depending on the previous natural aging, which strongly affects the mechanical characteristics in early post-welding days. The yield strength increases by 14% if the heat treatment is carried out after 3 days of natural aging while it decreases by 6% if carried out after 10 days. The ultimate tensile stress instead decreases in both but by different percentages, 6% and 18% for N3A and N10A, respectively.

In Fig. 7b, the evolution of the hardness for different aging conditions is shown. The influence of artificial aging on hardness in the nugget zone seems to be dependent on the previous natural aging. Comparing the effect of N3 and N3A treatments on the mean hardness in the nugget zone, an almost 15% increase can be observed. Contrarily, it decreases from N10 to N10A, with some similarities to yield stress. Then, regardless of the starting minimum hardness value in HAZ, the artificial aging reduces it due to overaging to almost 110 HV with a percentage reduction of 5% and 15% for N3A and N10A, respectively. Therefore, it is clear that artificial aging increases the hardness differential between the nugget and heat-affected zone passing from 18 and 31 HV in N3 and N10 to 40 and 41 HV for N3A and N10A.

The different mechanical behavior of specimens after artificial aging can be noticed in the sharp reduction of strain at break and the strain-softening before the rupture. The effect of the artificial aging in friction stir welded joints is affected by the previous natural aging. However, regardless of the different starting mechanical properties that depend on previous natural aging, PWHT produces similar mechanical properties for the joints.

3.3 Artificial aging and natural aging

Table 4 shows the mechanical properties of joints artificially aged and further exposed to natural aging.

The data show that artificial aging succeeded in stabilizing the mechanical properties with only a small reduction of 1% and 5% of UTS when comparing specimens belonging to category N3A with N3AN and N10A with N10AN. Both the minimum hardness and the average hardness in the nugget zone have been stabilized by artificial aging with changes lower than 2% detected after 45 days of natural aging, regardless of when the heat treatment was carried out (after 3 days or after 10 days).

Overall, artificial aging was proved effective in stabilizing the mechanical properties of the joint.

3.4 Temperature measurements

Table 5 summarizes all information about the thermal cycles. Information about TC_3 was not reported for WC_3 due to a positioning error during the experiment.

Table 3 Mechanical properties for N3, N3A, N10, and N10A specimens fabricated in the WC_3 configuration

WC	T	UTS (MPa)	Y (MPa)	ε_b (%)	HV_{HAZ} (HV0.5)	HV_{NZ} (HV0.5)
AA7075-T6		535	456	11	175	175
3	N3	374 ± 1	229 ± 1	8.6 ± 0.2	114	132 ± 1
3	N3A	351 ± 2	262 ± 3	3.6 ± 0.2	108	148 ± 5
3	N10	439 ± 6	286 ± 6	10.3 ± 0.7	124	155 ± 2
3	N10A	372 ± 3	269 ± 4	4.4 ± 0.2	109	150 ± 6

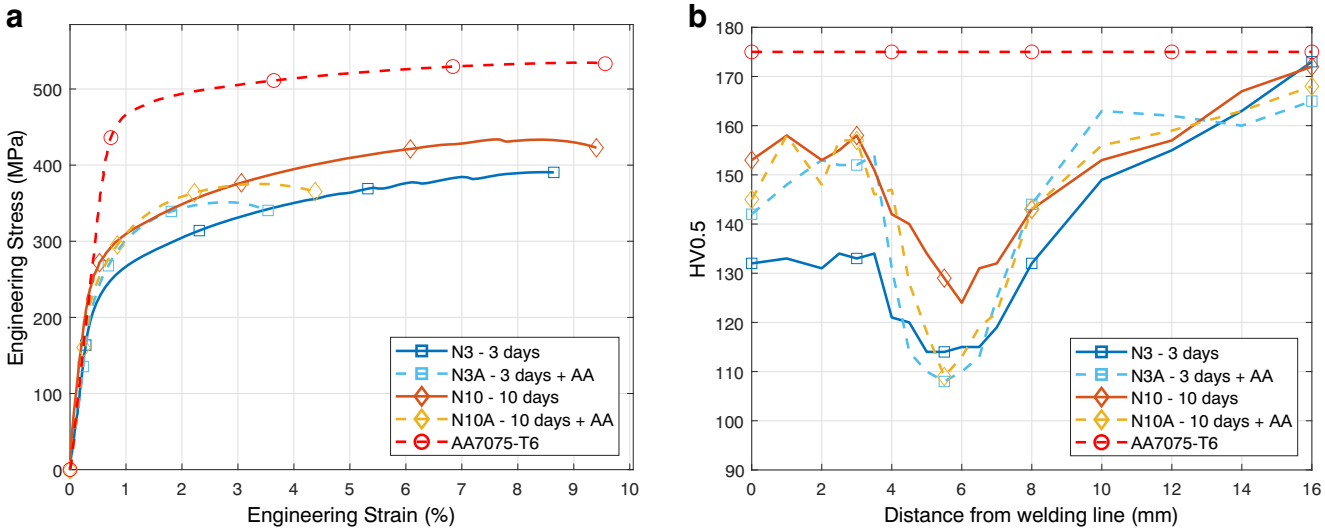

Fig. 7 **a** Engineering stress-strain curves and **b** hardness profiles for specimens N3, N3A, N10, and N10A made in the WC_3 configuration. Effect of the artificial aging on the mechanical properties

Comparing the temperature values recorded for the joints made in the WC_1 and WC_2, it is clear that almost the same thermal cycles have been obtained overall. Analyzing the maximum temperature values recorded in the closest zone to the nugget (TC_1), it is noteworthy that the tested configurations have guaranteed maximum temperatures close to 430 °C. The peak temperatures obtained with the closer thermocouple to the nugget zone suggest that similar peak temperatures were attained in the nugget zone independently of the welding configuration. The attainment of similar peak temperatures despite the different rotational speeds used is justified by the fact that different axial forces were employed. Also, it is known that aluminum alloys belonging to the 7xxx group are characterized by particularly low solidus temperature (477 °C for AA7075), which can be reached with relatively low rotational speeds below 1000 rpm [22]. The average grain size in the nugget zone was calculated using the linear intercept method. Six measurements for each micrograph have been made. It was estimated at 23 ± 5 µm for the longitudinally elongated grains in the base material and 3.4 ± 0.3 µm , 3.8 ± 0.45 µm, and 3.9 ± 0.69 µm for WC1, WC2, and WC3, respectively. The micrographs are displayed in Fig. 8 and only the samples subjected to a single type of aging (NA) were reported because no differences in grain size were observed after the post-welding heat treatment. Therefore, similar maximum temperatures reached in the NZ and the negligible effect of different cooling times on the NZ grain size can be confirmed, as already reported by [23]. Also, the differences in maximum temperature measured between TC_1 and TC_2 are around 20 °C and 50 °C for joints made at 60 mm/min and 180 mm/min, respectively. These measurements suggest steeper thermal gradients in the friction stir weld cross-section when higher feed rates are used.

Concerning the thermal cycles, comparing the heating and cooling rate values in Table 5, the significant influence of the welding speed is noticeable. Overall, the time elapsed above the temperature of 200 °C has approximately tripled in the lowest welding speed from 9 to 32 s for 180 mm/min and 60 mm/min. In addition, extra information can be gathered by estimating the different heat inputs obtained in

Table 4 Mechanical properties for N3A, N3AN, N10A, and N10AN specimens fabricated in the WC_3 configuration

WC –	T –	UTS (MPa)	Y (MPa)	ε_b (%)	HV_{HAZ} (HV0.5)	HV_{NZ} (HV0.5)
AA7075-T6		535	456	11	175	175
3	N3A	351 ± 2	262 ± 3	3.6 ± 0.1.7	108	148 ± 5
3	N3AN	346 ± 6	262 ± 6	3.6 ± 0	106	145 ± 1
3	N10A	372 ± 3	269 ± 4	4.4 ± 0.2	109	150 ± 6
3	N10AN	354 ± 2	269 ± 2	4.1 ± 0.2	109	150 ± 3

Table 5 Thermal cycle details for each welding configuration

WC	TC	Peak temperature (°C)	Heating rate (°C/s) (200 °C to peak)	Cooling rate (°C/s) (peak to 200 °C)	Heat input calculated from Eq. 1 (J/mm)
WC_1	TC_1	422	17	13	850.5
	TC_2	402	15	10	
	TC_3	346	13	8	
WC_2	TC_1	430	17	12	899.5
	TC_2	407	15	11	
	TC_3	350	14	9	
WC_3	TC_1	431	98	38	375.5
	TC_2	380	66	30	
	TC_3	NA	NA	NA	

the various configurations. The heat input was calculated using the empirical model proposed by [23] Eq. 1.

$$HI = 7.8\, v^{-0.80} \omega^{0.10} D_s^{0.55} d_p^{0.45} h_p^{0.3} \lambda^{0.4} \quad (1)$$

This empirical relationship considers the process parameters, welding speed v (mm/s) and rotational speed ω (rad/s), the tool geometry, shoulder diameter D_s (mm), pin diameter d_p (mm), pin height h_p (mm), and the thermal diffusivity of the base material λ (W/m·K). The estimated heat input is reported in Table 5 and seems to distinguish the joints carried out at different welding speeds. The higher welding speed results in low heat input and leads to steep thermal gradients moving away from the center and significantly shorter thermal cycles. Contrarily, different rotational speeds result in similar peak temperatures in the nugget zone, and their influence on heat input is much lower.

Thermal gradients on the upper surface of the welded plates were obtained with the IR camera. Since the sensor does not guarantee sufficient accuracy in this experimental configuration, the measured temperature trends were compared with those obtained from thermocouples. However, IR thermographic images enabled qualitatively observing the temperature distribution on the aluminum sheet and the harvesting of more information. Temperatures between 6 and 18 mm away from the welding line (AS) and 40 mm from the plunging point were recorded along time and then analyzed. The welding setup imposed the investigation zone because between the tool shoulder and the clamping system, only 12 mm is accessible from the IR camera, as shown in Fig. 9a. The choice of 40-mm distance from the plunging point ensured the steady-state of the process. The scheme to visualize the line of pixels analyzed in the frames acquired with the IR camera is shown in Fig. 9a. Figure 9b, c, and d are built assembling the temperature along the line for each time increment. They display the thermal gradient during the entire welding process of the marked zone represented by the red dotted line.

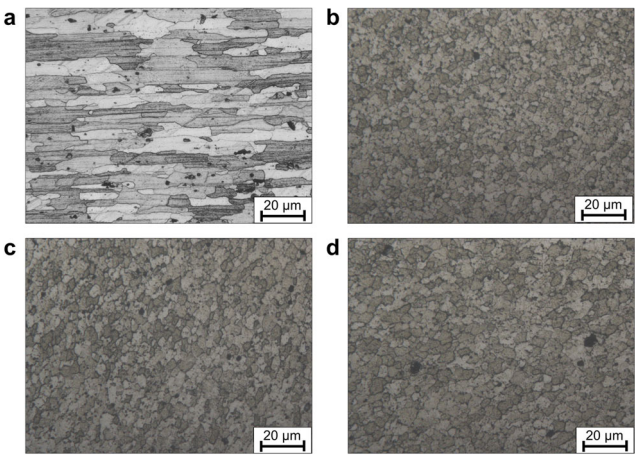

Fig. 8 Microscopic observation (× 50) in **a** base material and nugget zones: **b** WC_1: 60 mm/min–800 rpm–6 kN; **c** WC_2: 60 mm/min–1400 rpm–5.5 kN; **d** WC_3: 180 mm/min–1400–7.5 kN

The influence of the heat input on the thermal cycles is evident when comparing welds made with different welding speeds (Fig. 9b, c, with d), confirming what was observed with thermocouples. Contrarily, the extension of the heat-affected zone heated over 250 °C did not affect the heat input (Fig. 9b with c and d). These observations suggest that the extension of the heat-affected zone, at least as far as the upper surface of the welded plates is concerned, is affected by the rotational speed with about 2–3 mm extra extension of heated zones above 250 °C in joints made at 1400 rpm.

In summary, the welding configurations tested here can be divided for simplicity into two groups, high and low heat inputs. The influence of this quantity on the maximum temperature in the nugget zone was shown negligible. On the other hand, the duration of thermal cycles is significantly influenced by the heat input. Similarly, the steeper thermal gradient in the FSW section, intended as a faster decrease of temperature away from the center of the joint, was observed in lower heat input conditions. Hence, rather than the peak

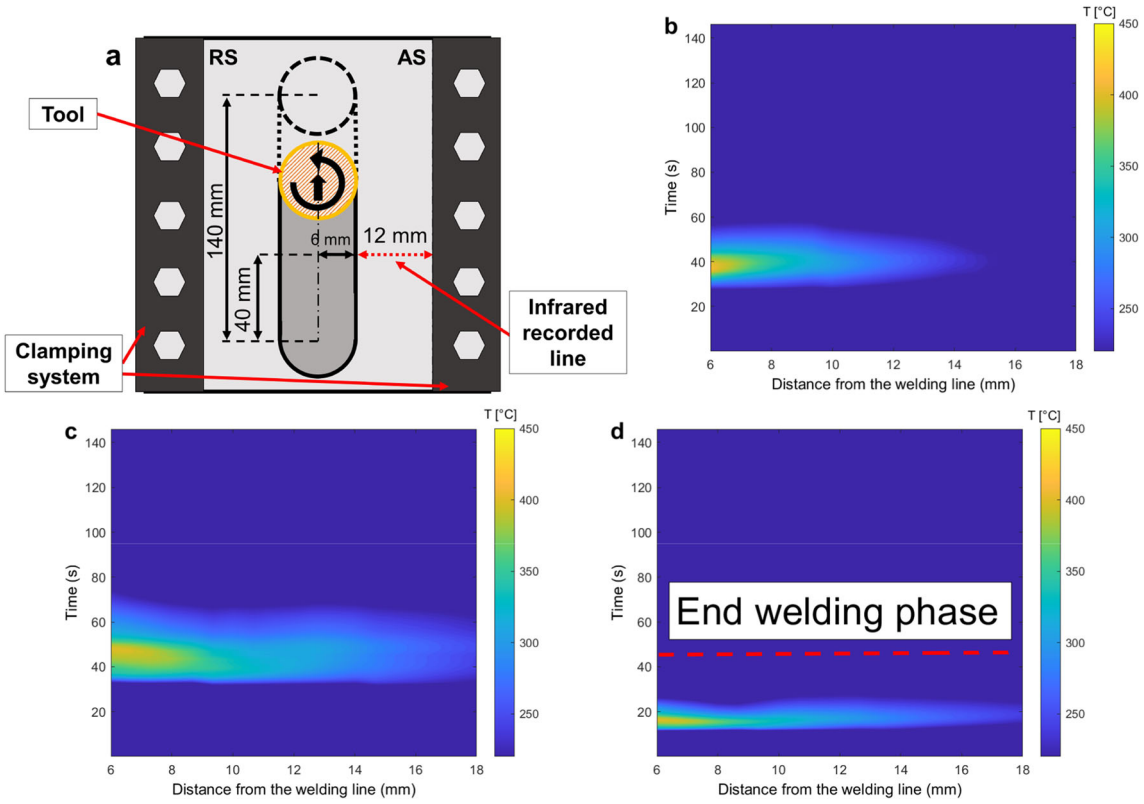

Fig. 9 **a** Scheme of the line of pixels (red dashed line 12 mm ≈ 19 pixels) on the AS analyzed in the IR frames. Temperature evolution with time: **b** WC_1, **c** WC_2, **d** WC_3

Fig. 10 Typical fracture locations of friction stir welding joints: **a** advancing side (+), **b** retreating side (-)

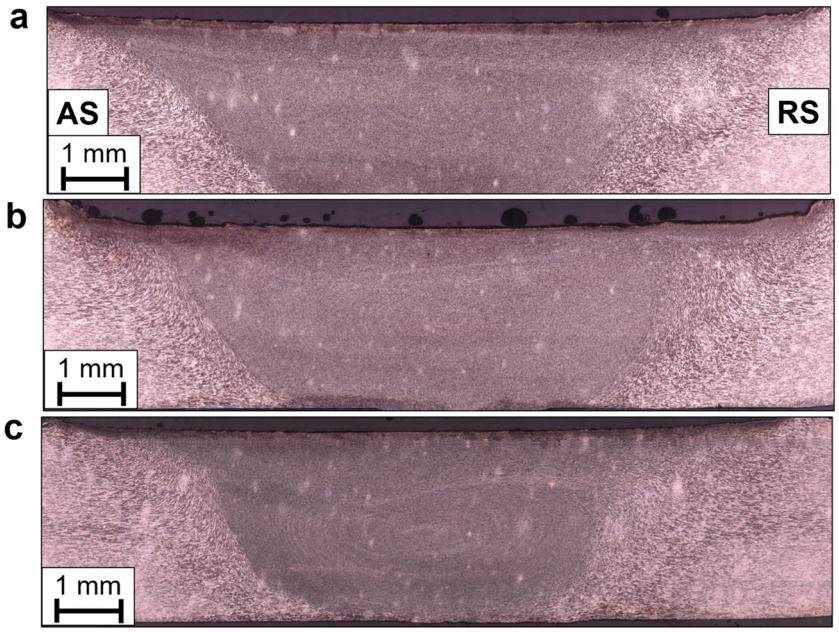

Fig. 11 Weld cross-section macrographs obtained with the different welding configurations: **a** WC_1, **b** WC_2, **c** WC_3

temperature, the heat input influences the duration and sharpness of the thermal cycle.

4 Discussion

The tested FSW joint specimens show mechanical properties strongly influenced by the process parameters reaching the best case the 84% and 66% of UTS and Y of the base material. The failure of the specimens occurred in the HAZ for all 63 tensile tests carried out with an equal percentage between AS (Fig. 10a) and RS (Fig. 10b). These results confirmed that the joints had no defects in the nugget zone and the absence of a precise rupture path on either side.

The cross-sections of the sound welds are displayed in Fig. 11.

Mechanical tests have shown the increase of the mechanical behavior of the specimens increasing the natural

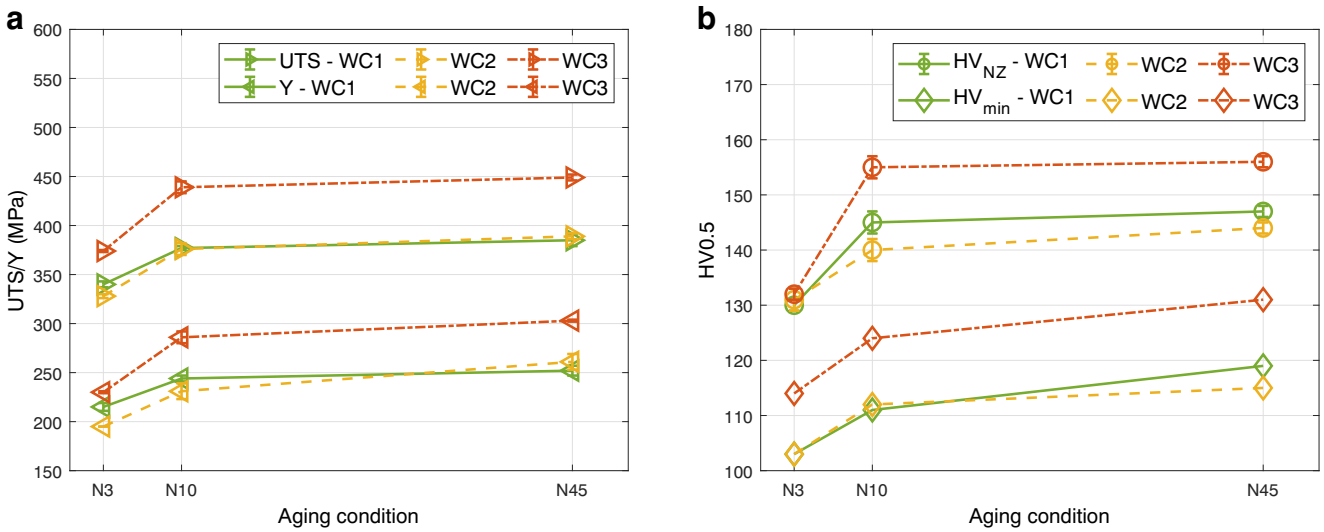

Fig. 12 Mechanical properties as a function of the aging condition for all the welds undergone natural aging: **a** ultimate tensile strength and yield strength, **b** hardness in the NZ, and minimum value in HAZ

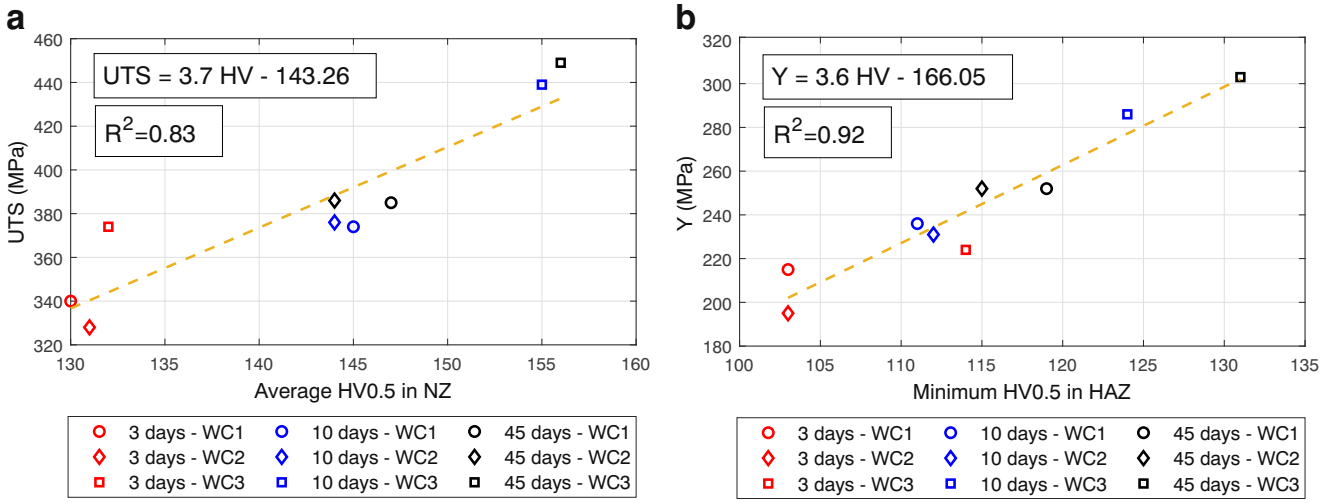

Fig. 13 Evolution of **a** ultimate tensile strength and **b** yield strength with the average hardness in the NZ and the minimum hardness in HAZ, respectively

aging time. Figure 12a and b display the UTS, Y, and HV_{NZ}, and HV_{min}, respectively, as a function of the natural aging for all the tested welding configurations.

The increase in mechanical properties is closely related to the results displayed in Fig. 12b, which shows the progressive increase in hardness in both NZ and HAZ with NA time. It is noteworthy that while UTS remains almost constant between 10 and 45 days of NA, Y continues to increase at least by 6%. This trend seems to agree with the hardness values in NZ and HAZ. Going from 10 to 45 days of NA, hardness in the nugget zone remains almost constant while the recovery in the heat-affected zones continues. Therefore, it would seem that the two quantities, UTS and Y, are directly affected by the hardness in NZ and HAZ, respectively. In Fig. 13, the first-order linear regression was adapted to both datasets with correlation coefficients R^2 .

The improvement of mechanical properties with natural aging is due to the recovery process in the various zones of the FSW joint, which varies according to the thermal shocks suffered during the process. The results in Fig. 12 indicate a distinction between the joints obtained with the two different welding speeds. The same remarkable distinction was pointed out by classifying the welding configurations according to the heat input. Figure 14 displays the mechanical properties of welds naturally aged for 45 days as a function of the heat input.

The decrease in the mechanical characteristics of the joints as the heat input increases is noticeable. Bearing in

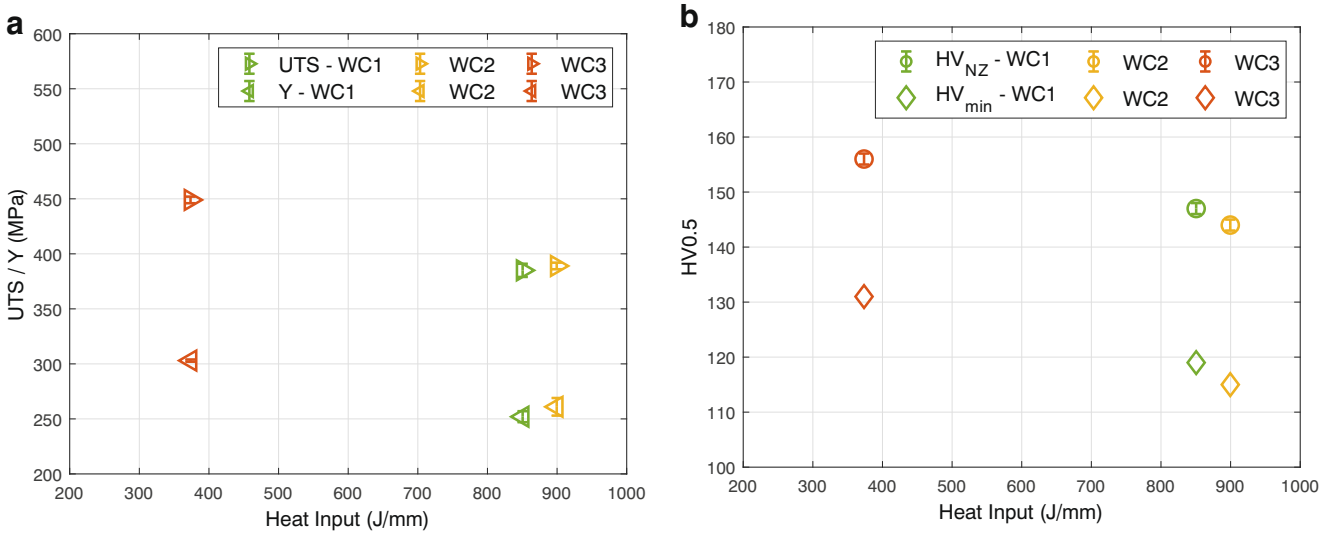

Fig. 14 Mechanical properties as a function of heat input for all the welds undergone 45 days of natural aging: **a** ultimate tensile strength and yield strength, **b** hardness in the NZ, and minimum value in HAZ

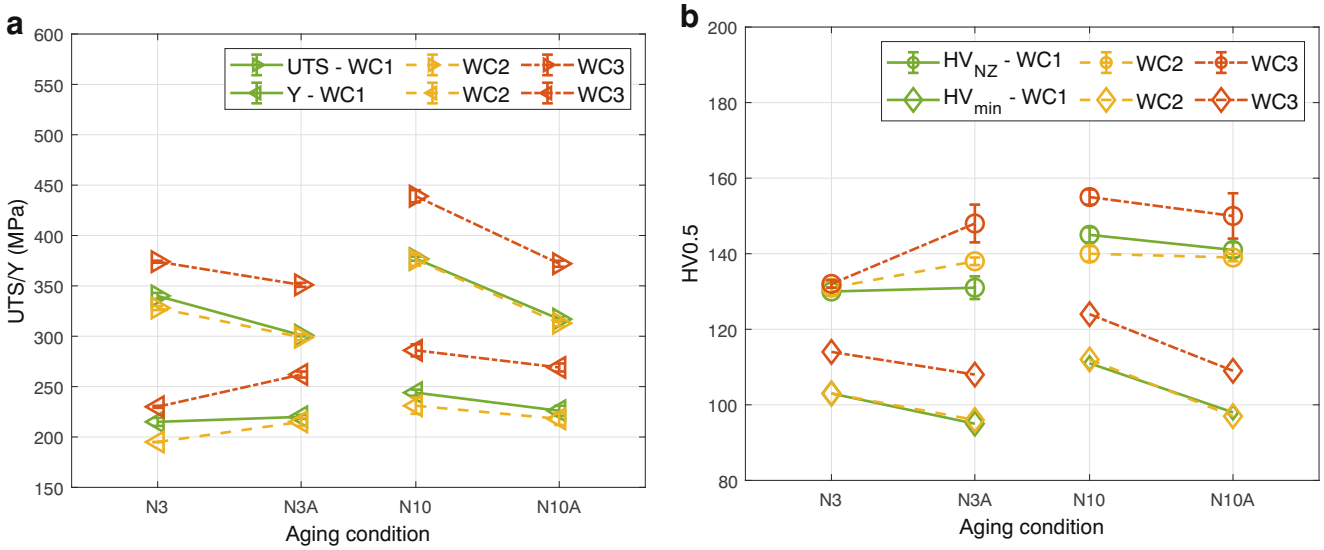

Fig. 15 Mechanical properties as a function of the aging condition for all the welds that have undergone natural aging and artificial aging: **a** ultimate tensile strength and yield strength, **b** hardness in the NZ, and minimum value in HAZ

mind that heat input mainly influences the thermal cycles, to explain such degradation of the mechanical properties, it is necessary to deepen the aspect of the precipitate population and its different evolution as a function of the heat input.

The high-strength AA7075-T6 is characterized predominantly by the presence of a dense system of finely distributed η' precipitates [24]. Friction stir welded joints belonging to this alloy degrade their mechanical properties due to the thermal cycles generated by the process that modify the initial precipitate population. In the nugget zone, a solution heat treatment of a few seconds takes place, the duration of which varies according to the welding speed, together with high strain rate that completely modifies the initial microstructure. Instead, the TMAZ is modified by the thermal cycle and severe plastic deformation, whereas the HAZ is only affected by the rapid rise and fall in temperature. Therefore, the three zones experience various phenomena, and different factors contribute to their final properties. The NZ characteristics are dictated by the fine equiaxed grains, the partial dissolution of η' and η precipitates in the matrix during the rapid solution heat treatment, the subsequent formation of η' and η during rapid cooling, and consequent NA [7]. In TMAZ, the high temperatures induce growth and rapid dissolution of metastable precipitates η' while grain deformation leads to strain hardening increasing the generation rate of dislocations [7]. The partial reduction in the strengthening precipitate density induces a decrease in strength, though partially recovered through increased dislocations. On the other hand, the HAZ microstructure is only modified by thermal cycles inducing the growth of metastable precipitates η' and the consequent reduction of the mechanical properties of those zones [6].

The comprehension of the results obtained in mechanical tests is closely related to the phenomena that occur in the NZ and HAZ during the process and natural aging. In the nugget zone, the rapid solution heat treatment and cooling lead to enough solute for solution strengthening and GP zone formation [25]. However, despite the difference in the duration of thermal cycles in the different configurations, hardness measured in the nugget zones at N3 is almost equivalent, as shown in Fig. 12b. On the contrary, by prolonging the natural aging time, the recovery of mechanical properties in the nugget zone seems to be affected by the heat input, with an increase of 20% and 10% for low and high heat input configurations. Strength recovery in the nugget zone with NA for heat-treatable aluminum alloy is justified with the longer time available for solution strengthening and GP zones formation after rapid cooling [11]. The microstructure of the nugget zone in AA7xxx is characterized by a high concentration of GP zones and fine equiaxed grains with different dislocation densities. Both are recognized as preferential nucleation sites for strengthening precipitates [7]. The final microstructure of the nugget zone is the result of a sequence of various complex phenomena, including continuous dynamic recrystallization favored by dynamic recovery [26]. Consequently, according to Su et al. [27], the fine equiaxed grains have different densities of dislocations, and they are in various degrees of recovery depending on each different thermo-mechanical history that occurred during FSW. The different heat inputs could have been responsible for the different degrees of recovery in the nugget zone grains. Therefore, the different evolution with natural aging may be justified as follows. Welding configuration with high heat input allowed a remarkable recovery

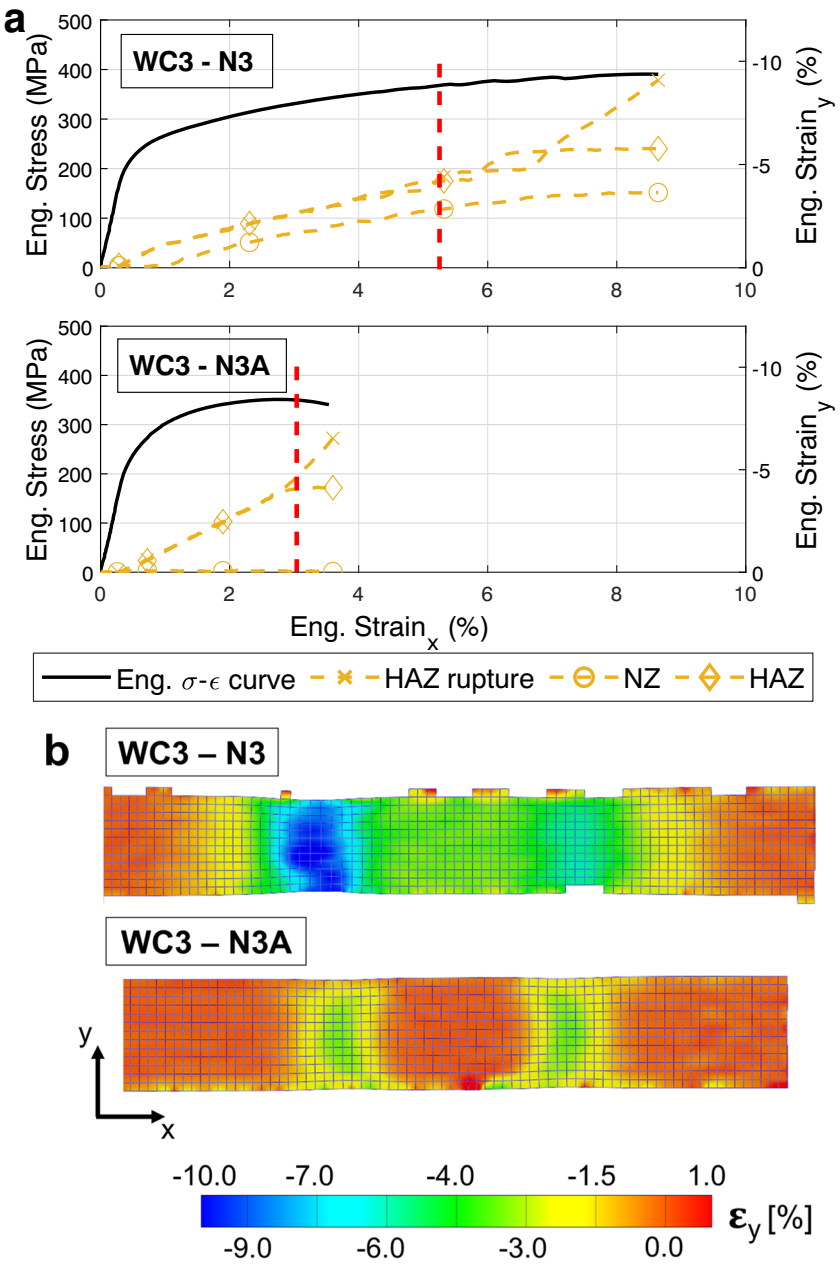

Fig. 16 Comparison among transverse strain ε_y in the different zones for WC_3 specimens in N3 and N3A aging conditions: **a** engineering stress and transverse strains ε_y as a function of longitudinal strain ε_x, **b** transverse strain ε_y gradients before fracture

with a decrease in dislocation densities and thus decreasing the concentration of nucleation sites for strengthening precipitation η'. This different recovery degree explains the increase in hardness in the nugget zone between N3 and N10, by 9, 15, and 23 HV for WC_2, WC_1, WC_3 ordered from the highest to the lowest heat input configuration. By further increasing exposure to natural aging, no significant difference can be observed in the evolution of recovery.

On the contrary, in the HAZ, the evolution of mechanical properties with natural aging seems to be mostly constant by comparing the various configurations while the strength depends on the heat input, and it is already evident from N3, as shown in Fig. 12b. These zones were recognized as the weakest for heat-treatable alloys due to the overaging, which leads to growth and partial dissolution of strengthening metastable precipitates η' and the formation of stable precipitates η [6]. Therefore, the weakness of the joint is due to the temperatures reached in HAZ, which, although significantly higher than the dissolution range of the strengthening precipitates η' between 180 and 260 °C [26], are not able to completely dissolve the latter. Hence, the weakening depends on the dissolution rate, which is related to the thermal cycle duration. This phenomenon, therefore, explains Fig. 14 and the clear difference in the mechanical properties of the joints as a function of the heat input. This result quantifies the direct correlation between

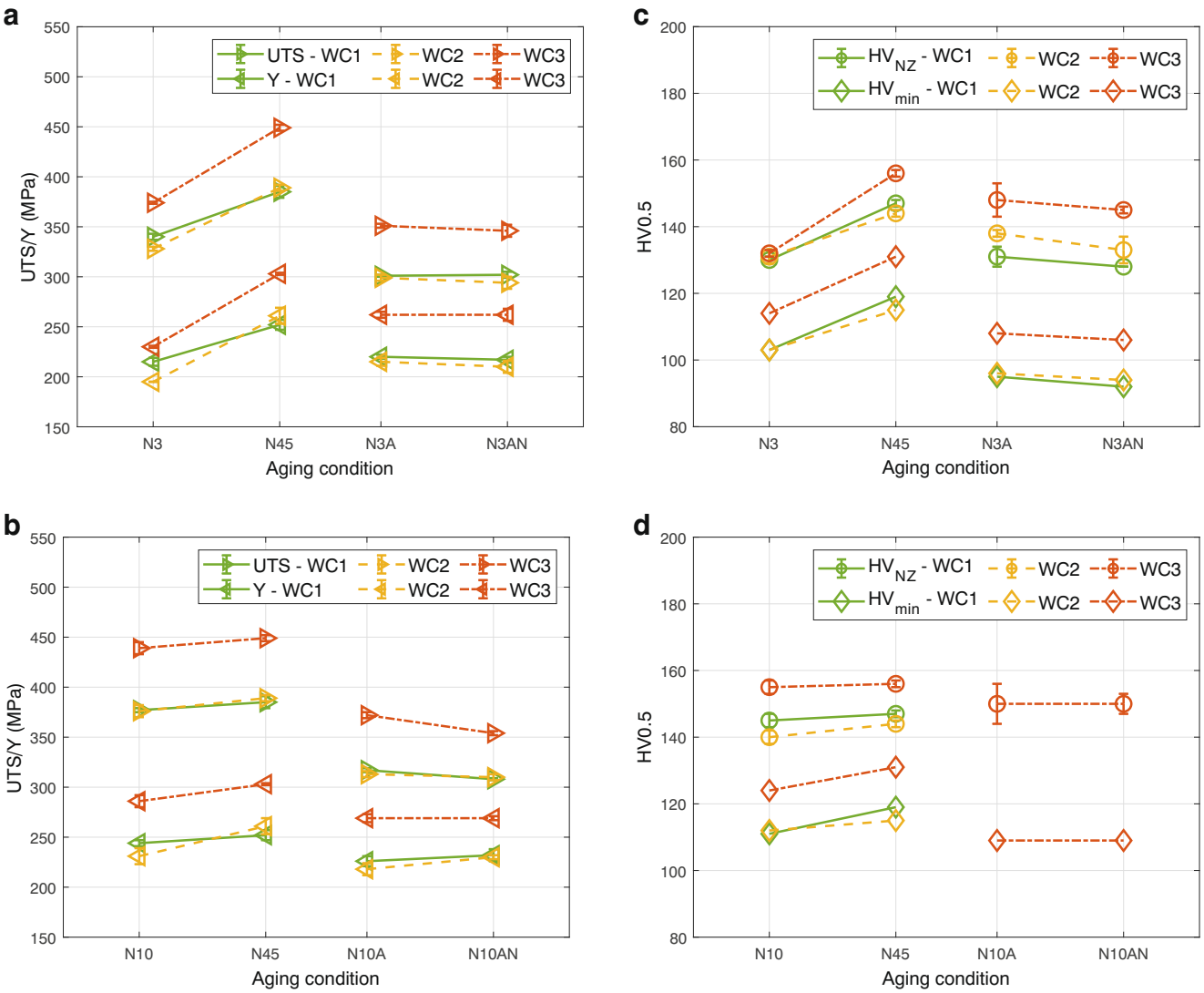

Fig. 17 Mechanical properties as a function of the aging condition for all the welds undergone natural aging, artificial aging, and subsequent further natural aging: **a**, **b** ultimate tensile strength and yield strength; **c**, **d** hardness in NZ, and minimum value in HAZ

the thermal cycles in HAZ and FSW joints' mechanical properties through the heat input. The overall increase in hardness with natural aging displayed in Fig. 12b is attributed to GP(II) nucleation followed by the formation of strengthening phase η' as the natural aging time increases [7].

In conclusion, the best mechanical properties of friction stir welds resulting from low heat input are related to higher recovery in the NZ due to the higher density of dislocations that operate as preferential nucleation sites of strengthening precipitates η' and to shorter thermal cycles in the HAZ that determines a lower rate of growth and dissolution of strengthening precipitates η'.

Figure 15a and b display UTS, Y, and HV_{NZ}, HV_{min}, respectively, as a function of the aging condition for specimens belonging to the group N3, N3A, N10, and N10A.

Among the effects of PWHT, two elements stand out. The former is the sharp reduction of the strain at break regardless of the welding configuration and the previous natural aging underwent by the specimens. The second is that while ultimate tensile strength and hardness in HAZ decrease in all cases, the evolution of yield strength and hardness in NZ depends on the natural aging before artificial aging. Specifically, specimens naturally aged for 3 days and then subjected to heat treatment (N3A) benefited from

artificial aging, while those that have undergone 10 days of natural aging before the artificial aging (N10A) experienced a decrease in yield strength and hardness in NZ.

Figure 16a shows the differences during tensile tests for specimens in the N3 and N3A aging conditions belonging to WC_3.

The engineering stress/strain curves show that in the configuration N3, there is instability with slight fluctuations in the curve at a certain point in the plastic regime. Similarly, in N3A, the reduction of strain at break is accompanied by strain-softening before the fracture. The onset of these two phenomena is highlighted in Fig. 16a by the dashed red lines. The evolution of transverse deformation ε_y in the nugget zone and the two heat-affected zones as a function of the longitudinal deformation ε_x for specimens under different aging conditions has been shown in Fig. 16a. This variable shows the strain localization effects in the different microstructural zones of the FSW joints. It turns out that in both cases, the two heat-affected zones deform equivalently up to a critical point where one of the two diverges until the breakage. However, the substantial difference lies in the different roles played by the nugget zone in the two tests. For N3, at least in the first half of the plastic regime, the deformation seems to be evenly distributed. Starting from the dashed red line, ε_y increasing rate decreases in the nugget zone, while in the two heat-affected zones, it first increases irregularly, and then one diverges from the other until the break. On the contrary, in the N3A configuration, the transversal deformation in the nugget zone is null. All the deformation is concentrated in the two heat-affected zones, thus inducing a much higher transversal deformation rate than N3, resulting in a much faster break. This behavior was observed in all artificially aged specimens. Therefore, the strain at break reduction for artificially aged specimens is explained with the strain localization in the HAZs. As shown in Fig. 16b, before the fracture, the transverse deformation is differently distributed in the two configurations. It is concentrated in two HAZ for N3A, whereas it is distributed along the gauge length for N3. This difference in artificially aged joints' mechanical behavior is due to the increased hardness difference in NZ and HAZ. This quantity was 18 and 40 HV in N3 and N3A, respectively, increasing the difference in mechanical behavior in the various zones of the joint that cause the strain localization in the weakest regions during tensile tests.

For the analysis of the impact of PWHT on mechanical properties according to previous natural aging, it is necessary to refer to the increase of the mechanical properties between N3 and N10. The most significant increase in mechanical properties occurs in the early days after welding. After 3 days of natural aging, the recovery of the mechanical properties of the various zones is still low. In the nugget zone, artificial aging speeds up the process that would have occurred through natural aging, accelerating the precipitation phenomenon due to the high concentration of solute available. The more pronounced increase in hardness in the nugget zone for low heat input configuration again relates to the higher dislocation density in the microstructure. Differently, after 10 days of natural aging, the PWHT lowered hardness in the nugget zone because the solute available was already precipitated. Then, the artificial aging causes the growth of the η' strengthening precipitates. On the other hand, in the HAZ, the hardness decreases because of the overaging that increases the growth of strengthening precipitates, independently from the previous natural aging. After 10 days, the higher recovery in the HAZ induces a more pronounced reduction in N10A compared to N3A. Overall, comparing the artificially aged friction stir welds' mechanical properties, the one previously naturally aged for 10 days gave slightly improved mechanical properties though lower than before heat treatment.

Thus, PWHT results in strain localization lowering strain at break. The positive effect of artificial aging on yield strength was achieved when the weld has undergone short previous natural aging. Otherwise, all mechanical properties worsen. Lastly, Fig. 17a, b, c, and d show the evolution of friction stir welds mechanical properties with extra natural aging after the post-welding heat treatment. By comparing the mechanical properties of the specimens tested immediately after artificial aging (N3A and N10A) and those that have been left to age naturally for another 45 days (N3AN and N10AN), it is clear that the mechanical properties have stabilized. Therefore, the post-welding heat treatment has proved to be effective for the stabilization of the mechanical properties with a variation in hardness, ultimate tensile strength, yield strength, and elongation at break always less than a few percentage points. However, comparing the mechanical properties of samples belonging to categories N3AN, N10AN, and N45, i.e., all those that have been exposed to aging for at least 45 days, it is clear that post-welding heat treatment, while stabilizing the mechanical properties, significantly reduces them in FSW AA7075-T6 joints. Table 6 shows the efficiency of the joint made in the WC3 under the aging condition N3AN,

Table 6 Joint efficiency for specimens belonging to N3AN, N10AN, and N45 and fabricated in the WC_3, i.e., 180 mm/min, 1400 rpm, 7.5 kN

WC_3	UTS	Y	ε_b
N3AN	65%	57%	44%
N10AN	66%	58%	44%
N45	84%	66%	96%

N10AN, and N45. The efficiency is defined as the ratio between the tensile properties (UTS, Y, and ε_b) of the FSW joints and the unwelded base material.

In conclusion, the heat treatment was effective in stabilizing the mechanical properties. The process parameters do not influence the evolution of the mechanical properties with artificial aging and the subsequent natural aging; thus, the heat provided does not affect the evolution of mechanical properties with aging. Nevertheless, the mechanical properties of joints subjected to artificial aging and then left to age naturally for 45 days are significantly lower than those aged only naturally for the same period.

5 Conclusion

This study examined the natural and artificial aging response of friction stir welded 7075-T6 fabricated with different welding parameters. The evolution of mechanical properties with aging has been correlated with welding parameters through heat input focusing on differences in nugget and heat-affected zone. Based on the present results, the following conclusions were pointed out.

1. Friction stir weld mechanical properties are maximized with the highest welding speeds reaching 84%, 66%, and 96% of UTS, Y, and ε_b of the BM. The influence of rotational speed was found to be negligible.
2. The influence of welding parameters on the mechanical properties was justified by microstructural modifications produced by the different heat input during welding. The joint with the best mechanical characteristics occurred in the lowest heat input configuration. Through temperature measurements, low heat input configurations, characterized by high welding speed, were shown to have the shortest duration of thermal cycles and the most severe temperature gradients moving away from the welding line. The strength in the nugget zone increases due to the lower dynamic recovery rate in the fine grains and consequently, higher dislocation densities that are preferential nucleation sites for strengthening precipitates during natural aging. In heat-affected zones, less time spent above the temperatures causing growth and dissolution of the strengthening precipitates guaranteed lower mechanical properties degradation.
3. Artificially aged joints show a drastic reduction in the strain at break, always below 5%. The cause was shown to be the increased hardness difference between NZ and HAZ that led to strain localization in the weak heat-affected zones. Conversely, in naturally aged welds, the deformation is distributed throughout the region between the two heat-affected zones, resulting in the higher strain at break, almost reaching the base material in the best welding configuration, with ε_b equal to 10.6%.
4. Independently of the degree of recovery of the mechanical properties after 3 and 10 days of natural aging, the effect of artificial aging allowed to obtain very similar mechanical properties comparing N3A and N10A. Although the specific impact of artificial aging on the friction stir welds varies depending on when it is carried out (N3 and N10), the final result is the homogenization of the mechanical properties at least in the time intervals tested in this work (N3A and N10A).
5. Post-welding heat treatments were proven to stabilize the mechanical properties of the FSW joint over the next 45 days of natural aging. However, mechanical properties are significantly lower (N3AN and N10AN) than the same joints subjected to natural aging (N45) with decreased ductility in all cases tested in this work by at least 40%.

Acknowledgments The authors want to thank Metallicadour for the production of the FSW joints and the IUT of Tarbes for the water jet cutting of specimens.

Funding This project received funding from the European Union's Marie Skodowska-Curie Actions (MSCA) Innovative Training Networks (ITN) H2020-MSCA-ITN-2017 under the grant agreement N°764979.

Appendix 1

Characteristics infrared camera

Table 7 Characteristics and parameters IR camera

Thermal resolution	20 mK at 30 °C
Frequency	50 Hz
Type sensor	50 mm
Numerical resolution	320 x 256 pixels
Estimated spatial resolution	0.66 x 0.79 mm
Wavelength scale measured	3.97 - 4.01 μm
Temperature range	200 - 500 °C
Integration time	87 μm
Type of detector	Indium

Calibration and data recording were managed by Altair software.

Appendix 2

Table 8 Mechanical properties for specimens fabricated with WC_1: 800 rpm–60 mm/min–6 kN

T –	UTS (MPa)	Y (MPa)	ε_b (%)	HV_{HAZ} (HV0.5)	HV_{NZ} (HV0.5)
N3	340 ± 3	215 ± 4	6.8 ± 0.6	103	130 ± 1
N10	377 ± 2	244 ± 3	7.8 ± 0.8	111	145 ± 2
N45	385 ± 6	252 ± 5	7.4 ± 0.6	119	147 ± 1
N3A	301 ± 1	220 ± 2	3.8 ± 0.1	95	131 ± 3
N10A	317 ± 2	226 ± 5	4.6 ± 0.1	98	141 ± 2
N3AN	302 ± 3	217 ± 3	4.6 ± 0.2	92	128 ± 0
N10AN	308 ± 1	232 ± 6	3.9 ± 0.2	NA	NA

Table 9 Mechanical properties for specimens fabricated with WC_2: 1400 rpm–60 mm/min–5.5 kN

T –	UTS (MPa)	Y (MPa)	ε_b (%)	HV_{HAZ} (HV0.5)	HV_{NZ} (HV0.5)
N3	328 ± 2	195 ± 1	7.6 ± 0.1	103	131 ± 2
N10	376 ± 6	231 ± 8	7.2 ± 0.5	112	140 ± 2
N45	390 ± 3	261 ± 8	7.7 ± 0.2	115	144 ± 1
N3A	299 ± 3	215 ± 4	4.1 ± 0.2	96	138 ± 1
N10A	313 ± 3	218 ± 6	4.7 ± 0.1	97	139 ± 1
N3AN	294 ± 6	210 ± 6	4.7 ± 0.3	94	133 ± 4
N10AN	310 ± 3	230 ± 2	4.5 ± 0.3	NA	NA

Table 10 Mechanical properties for specimens fabricated with WC_3: 1400 rpm–180 mm/min–7.5 kN

T –	UTS (MPa)	Y (MPa)	ε_b (%)	HV_{HAZ} (HV0.5)	HV_{NZ} (HV0.5)
N3	374 ± 1	229 ± 1	8.6 ± 0.2	114	132 ± 1
N10	439 ± 6	286 ± 6	10.3 ± 0.7	124	155 ± 2
N45	449 ± 3	303 ± 1	10.6 ± 0.3	131	156 ± 1
N3A	351 ± 2	262 ± 3	3.6 ± 0.1	108	148 ± 5
N10A	372 ± 3	269 ± 4	4.4 ± 0.2	109	150 ± 6
N3AN	346 ± 6	262 ± 6	3.6 ± 0.1	106	145 ± 1
N10AN	354 ± 3	269 ± 2	4.1 ± 0.2	109	150 ± 3

References

1. Threadgill PL, Leonard AJ, Shercliff HR, Withers PJ (2009) Friction stir welding of aluminum alloys. Int Mater Rev 54:2:49–93. https://doi.org/10.1179/174328009X411136
2. Ericsson M, Sandstrom R (2003) Influence of welding speed on the fatigue of friction stir welds, and comparison with MIG and TIG. Int J Fatigue 25(12):1379–1387. https://doi.org/10.1016/S0142-1123(03)00059-8
3. Nelson TW, Steel RJ, Arbegast WJ (2003) In situ thermal studies and post-weld mechanical properties of friction stir welds in age hardenable aluminum alloys. Sci Technol Weld Join 8(4):283–288. https://doi.org/10.1179/136217103225011005
4. Hossfeld M (2019) Time-dependency of mechanical properties and component behavior after friction stir welding. Int J Adv Manuf Technol 102(5-8):2297–2305. https://doi.org/10.1007/s00170-019-03324-x
5. Zhang X, Chen Y, Hu J (2018) Recent advances in the development of aerospace materials. Prog Aerosp Sci 97:22–34. https://doi.org/10.1016/j.paerosci.2018.01.001
6. Mahoney MW, Rhodes CW, Flintoff JG et al (1998) Properties of friction-stir-welded 7075 t651 aluminum. Metall Mater Trans A Phys Metall Mater Sci 29(7):1955–1964. https://doi.org/10.1007/s11661-998-0021-5
7. Fuller CB, Mahoney MW, Calabrese M, Micona L (2010) Evolution of microstructure and mechanical properties in naturally aged 7050 and 7075 Al friction stir welds. Mater Sci Eng A 527(9):2233–2240. https://doi.org/10.1016/j.msea.2009.11.057
8. Jamshidi Aval H, Serajzadeh S (2014) A study on natural aging behavior and mechanical properties of friction stir-welded AA6061-t6 plates. Int J Adv Manuf Technol 71(5-8):933–941. https://doi.org/10.1007/s00170-013-5531-7
9. Sato YS, Kokawa H, Enomoto M et al (1999) Precipitation sequence in friction stir weld of 6063 aluminum during aging. Metall Mater Trans A: Phys Metall Mater Sci 30(12):3125–3130. https://doi.org/10.1007/s11661-999-0223-5
10. Jandaghi MR, Badini C, Pavese M (2020) Dissimilar friction stir welding of AA2198 and AA7475: Effect of solution treatment and aging on the microstructure and mechanical strength. J Manuf Process 57:712–724, 1526–6125. https://doi.org/10.1016/j.jmapro.2020.07.037
11. Sharma C, Dwivedi DK, Kumar P (2013) Effect of post weld heat treatments on microstructure and mechanical properties of friction stir welded joints of Al-Zn-Mg alloy AA7039. Mater Des 43:134–143. https://doi.org/10.1016/j.matdes.2012.06.018
12. Mishra RS, Komarasamy M (2016) Friction stir welding of high strength 7XXX aluminum alloys. Butterworth-Heinemann, Denton, Texas
13. Dong P, Li H, Sun D et al (2013) Effects of welding speed on the microstructure and hardness in friction stir welding joints of 6005A-T6 aluminum alloy. Mater Des 45:524–531. https://doi.org/10.1016/j.matdes.2012.09.040
14. Golezani A.S., Barenji R.V., Heidarzadeh A. et al (2015) Elucidating of tool rotational speed in friction stir welding of 7020-T6 aluminum alloy. Int J Adv Manuf Technol 81:1155–1164. https://doi.org/10.1007/s00170-015-7252-6
15. Rajakumar S, Muralidharan C, Balasubramanian V (2011) Influence of friction stir welding process and tool parameters on strength properties of AA7075-t6 aluminum alloy joints. Mater Des 32(2):535–549. https://doi.org/10.1016/j.matdes.2010.08.025
16. Tabasi M, Farahani M, Givi MKB et al (2016) Dissimilar friction stir welding of 7075 aluminum alloy to AZ31 magnesium alloy using SiC nanoparticles. Int J Adv Manuf Technol 86:705–715. https://doi.org/10.1007/s00170-015-8211-y
17. Moharami A, Razaghian A, Babaei B et al (2020) Role of Mg2Si particles on mechanical, wear, and corrosion behaviors of friction stir welding of AA6061-t6 and Al-Mg2Si composite. J Compos Mater 54(26):4035–4057. https://doi.org/10.1177/0021998320925528
18. Zhang J, Feng XS, Gao JS et al (2018) Effects of welding parameters and post-heat treatment on mechanical properties of friction stir welded AA2195-t8 Al-Li alloy. J Mater Sci Technol 34(1):219–227. https://doi.org/10.1016/j.jmst.2017.11.033
19. Ambrosio D, Wagner V, Garnier C et al (2020) Influence of welding parameters on microstructure, thermal field and defect formation in AA7075-t6 friction stir welds. Weld World 64:773–784. https://doi.org/10.1007/s40194-020-00869-4
20. Staley JT (1974) Aging kinetics of aluminum alloy 7050. Metall Trans 5(4):929–932
21. ASTM E8M-04 Standard test methods for tension testing of metallic materials (Metric)
22. Long T, Tang W, Reynolds AP (2007) Process response parameter relationships in aluminum alloy friction stir welds. Sci Technol Weld Join 12(4):311–317. https://doi.org/10.1179/174329307X197566
23. Yi D, Onuma T, Mironov S et al (2017) Evaluation of heat input during friction stir welding of aluminum alloys. Sci Technol Weld Join 22(1):41–46. https://doi.org/10.1080/13621718.2016.1183079
24. Loffler H, Kovacs CSI, Lendvai J (1983) Review Decomposition processes in AI-zn-mg alloys. J Mater Sci 18:2215–2240
25. Reynolds AP, Tang W, Khandkar Z et al (2005) Relationships between weld parameters, hardness distribution and temperature history in alloy 7050 friction stir welds. Sci Technol Weld Join 10(2):190–199. https://doi.org/10.1179/174329305X37024
26. Su JQ, Nelson TW, Mishra R et al (2003) Microstructural investigation of friction stir welded 7050-T651 aluminum. Acta Mater 51(3):713–729. https://doi.org/10.1016/S1359-6454(02)00449-4
27. Su JQ, Nelson T, Sterling JC (2005) Microstructure evolution during FSW/FSP of high strength aluminum alloys. Mater Sci Eng A 405(1-2):277–286. https://doi.org/10.1016/j.msea.2005.06.009